

# Phase and mechanical property prediction of intermetallic-strengthening Ti-Al-Cr-Nb-Ni-Cu-Co high entropy alloys by thermo-physical parametric calculation and CALPHAD-based technique

Ufoma Silas Anamu<sup>1</sup>, Olusoji Oluremi Ayodele<sup>1</sup>, Emmanuel Olorundaisi<sup>1</sup>, Bukola Joseph Babalola<sup>1</sup>, Peter Ifeolu Odetola<sup>1</sup>, Anthony Ogunmefun<sup>1</sup>, Kingsley Ukoba<sup>2</sup>, Tien-Chien Jen<sup>2</sup>, Peter Apata Olubambi<sup>1</sup>

<sup>1</sup>Centre for Nanoengineering and Advanced Materials, School of Mining, Metallurgy and Chemical Engineering, University of Johannesburg, Johannesburg 2092, South Africa.

<sup>2</sup>Department of Mechanical Engineering Science, University of Johannesburg, South Africa

\*Corresponding author: [usanamu7@gmail.com](mailto:usanamu7@gmail.com)

**Abstract.** Non-conventional alloy developmental approach targeted at incorporating intermetallics as strengtheners using thermo-physical parametric calculation and CALPHAD-based tool (ThermoCalc software) were adopted in the design of septenary non-equiatom [Ti<sub>20</sub>Al<sub>20</sub>Cr<sub>5</sub>Nb<sub>5</sub>Ni<sub>19</sub>Cu<sub>12</sub>Co<sub>19</sub>] HEAs. Thermo-physical properties indicated a lightweight and dual-phase HEA having density of 6.22gcm<sup>-3</sup> and 6.88 VEC value. At room temperature conditions, computation using ThermoCalc of version 2021b (TCHEA4) encrypted database shows the presence of 6 phases, where BCC\_B2, FCC\_L12, Sigma, Heusler and C1\_Laves are pronounced at varied volume fractions with BCC\_B2 occupying 69.8 vol% of the predicted HEA. Traces of O\_Phase were observed, and 144.096HV was computed as the maximum predicted total hardness.

**Keywords:** High entropy alloys, thermo-physical parametric calculations, CALPHAD-based method, ThermoCalc software, intermetallic-strengthening,

## 1. Introduction

Traditionally, alloy creation involves a base metal chemically combined with small quantities of one or, seldom, two alloying elements, for example, iron with other minor alloys in steel manufacturing, or nickel with the addition of other alloying elements in superalloys. This method has effectively improved the bulk characteristics of alloys [1], while the parent metal maintains its primary phase. A significant transformation in materials science has emerged with the introduction of high entropy alloys (HEAs), wherein five or more constituent elements are combined in approximately equal proportions, leading to the creation of a new materials system characterized by an exceptional blend of properties derived from all constituent elements [2,3].

HEAs are superior to typical alloys because of their relatively high configurational entropy and specific traits known as "the core effects," which include the cocktail/synergetic, slow diffusion, and crystal lattice-distortion effects. They are also capable of driving simple solid-solution phases [4], demonstrating extraordinary properties like high strength, enhanced resistance to chemical attack at elevated temperatures, great thermal stability, and superior wear resistance [5].

The fundamentally simple microstructures that characterize the HEAs are dictated by the simple solid-solution phases such as the hexagonal close-packed (HCP), face-centered cubic (FCC), body-centered cubic (BCC), or even a combination of any. These typical basic microstructures are believed to be driven by the alloy's mixing entropy ( $\Delta S_{mix}$ ). Nevertheless, recent studies have shown that additional thermodynamic and geometrical parameters are also important for the stability of the simple solid-solution phases in HEAs. These parameters, which include the valence electron concentration (VEC), the atomic size difference ( $\delta$ ) [6], the enthalpy of mixing ( $\Delta H_{mix}$ ), and the impacts of the interacting  $\Omega$ -parameter [7,8], are very essential in the determination of the stability of solid-solution phases in HEAs

[9–11].

The hypothesis behind the search for simple solid-solution alloys is sometimes supported by the claim that the alloys are resilient and retain ductility and damage tolerance while intermetallic (IM) phases are believed to result in material embrittlement and complicated processing. This is perhaps a bit of an oversimplification of the situation. Alloys can be embrittled by IM formation, however this is not always the case. Practically, most advanced structural alloys, including superalloys (for which the IM phase is typically the biggest proportion by volume), pearlitic steels, and age-hardened aluminium alloys, can contain IM structures intentionally as the major microstructural components. The exceptional combination of strength and damage tolerance in such IM-containing alloys is the result of meticulous control of the size, volume fraction, shape, and distribution of the IM phases [9,12].

In recent times, researchers have ventured into the design and fabrication of high entropy intermetallics (HEIs) materials otherwise referred to as intermetallic-strengthening high entropy alloy as a viable alternative with better mechanical characteristics to the simple solid-solution HEAs, by investigating the benefits of the mechanism of particle strengthening driven by the precipitation of a second or more IM phase(s) in the HEAs system (particularly in lightweight HEAs), to balance the strength-to-density ratio without necessarily causing materials embrittlement. Hence, taking off from HEAs, HEIs are identified as one of the evolving materials for the future for advanced performance in various engineering applications [13,14]. Generally, intermetallic-containing alloys benefit from lightweightness, great specific strength, elevated temperature and corrosion resistance capabilities that find application in the aerospace, energy storage and automotive to mention but a few [15–18].

In light of the growing demand for novel materials with an appreciable balance in strength, ductility, lightweight and high-temperature capability, this research was borne by appropriating a design concept involving the use of thermo-physical parametric calculations and CALPHAD-based method to simulate and predict the phase and thermo-mechanical properties of intermetallic-containing HEAs for structural and high-temperature applicability.

## **2. Research methodology**

### **2.1 Design conditions and basis for HEAs for thermo-mechanical applications**

Anamu et al. 2023 [15], in previous research reviewed in detail the fundamental concept for designing HEAs that can be employed for both structural and elevated temperature domains. As corroborated by literature, recommendations for the design of HEIs for thermo-mechanical applications must be materials that are capable of satisfying both structural and high-temperature demands. This includes:

- Lightweight property HEA (density  $< 7 \text{ g.cm}^{-3}$  [19]),
- High-strength property HEA (intermetallic phase(s) as strengtheners [15]), and
- High-temperature ability (with usable temperature  $T_{ref} \geq 1373 \text{ K}$  [20]).

### **2.2 Material selection in the design of HEAs for thermo-mechanical applications**

The performance of any material in service fundamentally depends on the properties of the material system prompted by the choice of the raw/starting materials selected for its manufacturing or processing route [21]. In this study, elements comprising Ti, Al, Cr, Nb, Ni, Cu, and Co were carefully selected as suggested by literature as choice materials following their individual properties [15], and the potential combinatorial features they will effect for thermo-mechanical application.

### **2.3 Thermo-physical parametric calculation**

Just as the Hume-Rothery law to conventional alloy design, knowledge of the thermodynamic and physical properties (see Table 1) is very key to modelling and predicting the nature of non-conventional alloys (high entropy alloys) prior

to the actual production process [15,18,22,23].

**Table 1:** Thermo-physical parameters for solid–solution HEAs

Parameters	Equations	Condition	References
Mixing entropy ( $\Delta S_{mix}$ )	$-R \sum_{i=1}^n (c_i \ln c_i)$	$11 \leq \Delta S_{mix} \leq 19.5 \text{ J}/k.mol$	[24]
Electronegativity difference ( $\Delta\chi$ )	$\sqrt{\sum_{i=1}^n c_i (x_i - \sum_{j=1}^n c_j x_j)^2}$	$\Delta\chi < 6\%$	[9,25]
Mixing enthalpy ( $\Delta H_{mix}$ )	$\sum_{i=1, i \neq j}^n \Omega_{ij} c_i c_j$	$-22 \leq \Delta H_{mix} \leq 7 \text{ kJ}/mol$	[26]
Atomic size mismatch ( $\delta$ )	$100 \sqrt{\sum_{i=1}^n c_i (1 - \frac{r_i}{r_a})^2}$	$\delta < 6.5\%$	[25,26]
Valence electronic configuration (VEC)	$\sum_{i=1}^n c_i (VEC)_i$	$VEC \geq 8.0$ for FCC $VEC < 6.87$ for BCC	[9]
Interacting parameter ( $\Omega$ )	$\frac{T_m \Delta S_{mix}}{ \Delta H_{mix} }$	$\Omega > 1$	[27]
Melting temperature ( $T_m$ )	$\sum_{i=1}^n c_i (T_m)_i$		[26,28]

The various items used are defined thus- where  $C_i(C_j)$  is the atomic percentage of the  $i$ -th( $j$ -th) component.  $r_i$  is the atomic radius.  $(VEC)_i$  is the valence electron concentration.  $\chi$  is the Pauling electronegativity.  $T_m$  is the calculated melting point through the atomic percentage.  $\Delta G_{max}$  is the lowest (intermetallic) or highest (segregated) possible Gibbs free energy from the formation of binary systems.

From the knowledge of the thermo-physical data, inferences can be drawn to state if the proposed material is actually a mono phase - BCC or FCC or a dual phase system of alloy by calculating the valence electron configuration (VEC). Thermo-physical parameters can also be insightful in suggesting if the HEA formed is a disordered solid solution type or an ordered solid solution containing either an intermetallic or amorphous structure(s).

## 2.4 CALPHAD-based simulation technique

2021b version of the ThermoCalc software encrypted with thermodynamic database (TCHEA4) for high entropy alloy was used to calculate the phase diagram, phase quantification, stable phases and for prediction of the mechanical properties of the HEA. The Phase Diagram module of the software was explored for computing the phase diagram of the alloy at a pre-set range of temperature and composition. Quantification of the phases present was thereafter computed using the Single Point Equilibrium module of the ThermoCalc software, whereas the One Axis Equilibrium module was accessed for identifying the stable phases present at specific temperatures. Prediction of the mechanical properties was performed using the Property Model Calculator (PMC) module of the software.

### 3. Results and discussion

#### 3.1 Thermo-physical properties of the designed $\text{Ti}_{20}\text{Al}_{20}\text{Cr}_5\text{Nb}_5\text{Ni}_{19}\text{Cu}_{12}\text{Co}_{19}$ HEA

From manual calculation [15,18], which was also confirmed using high entropy alloy predicting software (HEAPS) [29], the thermo-physical parametric equations in Table 1 were used as an optimization tool to compute the thermo-physical properties of an array of alloys that satisfy the pre-condition of lightweightness, high strength and high-temperature capability and resulted in a non-equiatomic ( $\text{Ti}_{20}\text{Al}_{20}\text{Cr}_5\text{Nb}_5\text{Ni}_{19}\text{Cu}_{12}\text{Co}_{19}$ ) HEA. Table 2 depicts the results obtained for the HEA.

**Table 2.** Thermo-physical properties of designed HEA

Nominal $\rho$ ( $\text{gcm}^{-3}$ )	Structure	VEC	$\Delta H_{mix}$ ( $\text{kJmol}^{-1}$ )	$\Delta S_{mix}$ ( $\text{kJmol}^{-1}$ )	$T_m$ ( $^{\circ}\text{C}$ )	$\delta$ (%)	$\Omega$	$\Delta x$
6.2176	BCC + FCC	6.88	-21.05	15.205	1376	6.01	1.17	1.741

Following Table 2, there is the possibility of designing solid-solution HEAs since the various values obtained for all the thermo-physical parameters lie within the phenomenological ranges for the formation of solid-solution HEAs as stipulated in Table 1. The VEC value depicts a HEA with a dual phase that comprises BCC and FCC structures. In addition, the nominal density measures to  $6.2176 \text{ gcm}^{-3}$ , and this indicates that the HEA can be classified as lightweight multicomponent system [19].

Thermo-physical parametric calculation has been adjudged a statistically dependent approach that lacks scientific fundamentality, and its inability to provide further information on the phase quantification, and the specific type of intermetallic phases formed. Notwithstanding, it is considered as a preliminary strategy in the design of multicomponent alloys that can be supplemented by the incorporation of CALPHAD-based technique which is capable of providing sufficient information for modelling of phase diagram, and this serves as a GPS or Map in the design of multicomponent alloys.

#### 3.2 Thermodynamic simulation of the phase diagram, phases present and phase quantification of $\text{Ti}_{20}\text{Al}_{20}\text{Cr}_5\text{Nb}_5\text{Ni}_{19}\text{Cu}_{12}\text{Co}_{19}$ HEA

With the aid of ThermoCalc software, the temperature versus composition (T-C) phase diagram represented in Figure 1 was computed for the septenary non-equiatomic HEA using the Phase Diagram module. At a pressure of 1bar, and temperature range between  $0^{\circ}\text{C}$  and  $1800^{\circ}\text{C}$ , chemical reactions across the isopleth line (indicated with red vertical broken lines) that corresponds to the HEA ( $\text{Ti}_{20}\text{Al}_{20}\text{Cr}_5\text{Nb}_5\text{Ni}_{19}\text{Cu}_{12}\text{Co}_{19}$ ) show the formation of complex phases reported in Table 3.

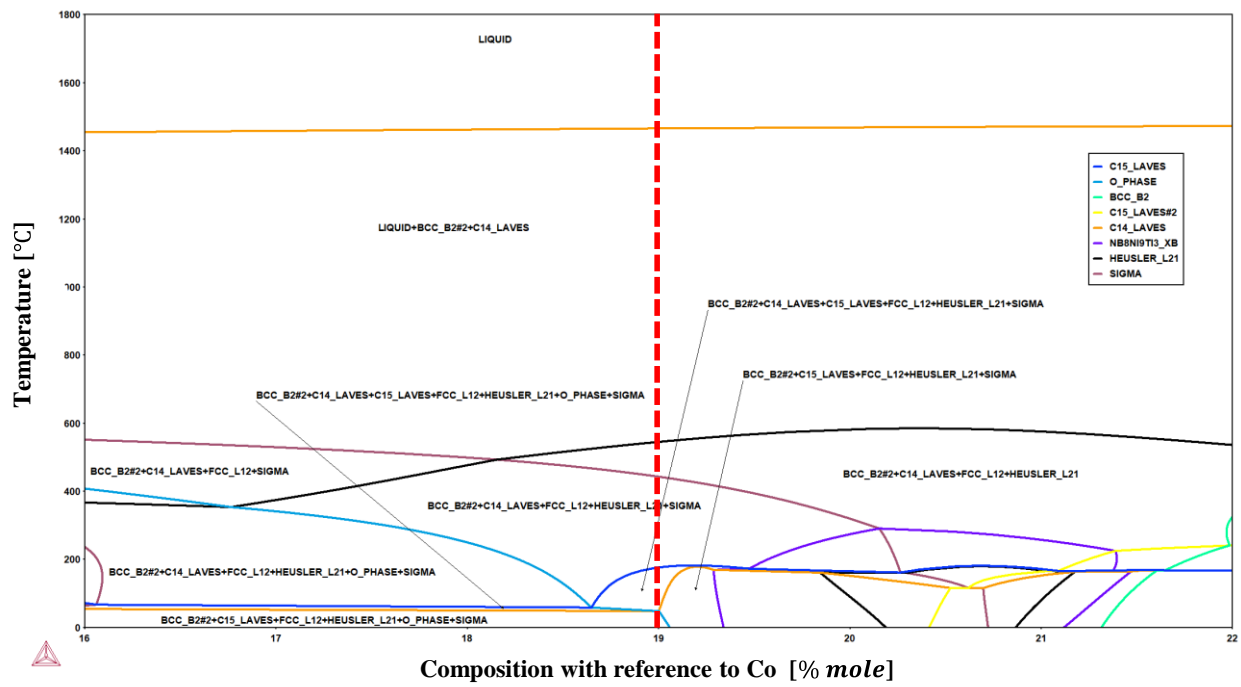


**Fig. 1:** T-C phase diagram of non-eutotoxic  $Ti_{20}Al_{20}Cr_5Nb_5Ni_{19}Cu_{12}Co_{19}$  HEA

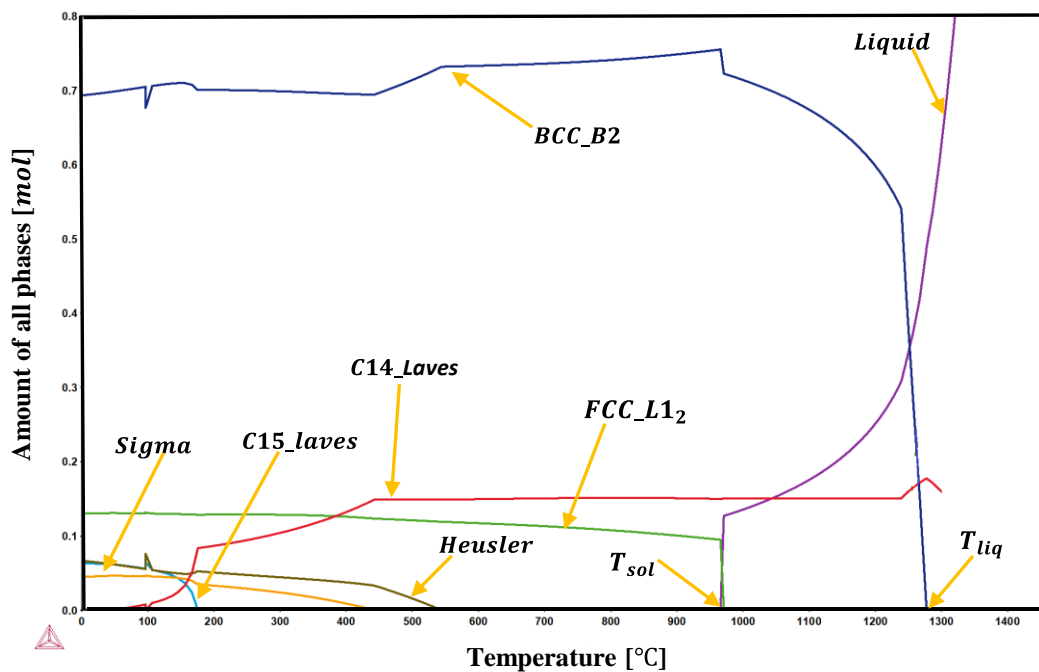


**Fig. 2:** Amount of all phases in  $Ti_{20}Al_{20}Cr_5Nb_5Ni_{19}Cu_{12}Co_{19}$  HEA

Figure 2 shows the stable phases in the designed HEA computed from the One Axis Equilibrium module of the ThermoCalc software. It can be predicted that at ambient temperature, BCC at 69.6-mole percentage exists as the predominant phase. BCC crystals also exhibit the longest stability from 1276 °C to room temperature ( $T_{room}$ ). Stable phases besides the BCC are FCC\_L2<sub>1</sub>, Heusler\_L2<sub>1</sub>, Sigma, Laves and the O\_phase, with their respective phase quantification, elemental constituents and temperature ranges reported in Table 3.

Additional features in Figure 2 are the liquidus temperature ( $T_{liq}$ ) and solidus temperature ( $T_{sol}$ ) computed as 1276 °C and 965 °C respectively from the ThermoCalc thermodynamic simulation. The value obtained for  $T_{sol}$  is very critical as it serves as a guide for the processing temperature of the designed HEA. In the case of spark plasma sintering, processing at a temperature above 965 °C will result in liquid melt interference that can lead to damage of the sintering die. Hence, for the sake of safety and quality production process, reasonable temperature clearance must be maintained.

**Table 3.** ThermoCalc predicted features for Ti<sub>20</sub>Al<sub>20</sub>Cr<sub>5</sub>Nb<sub>5</sub>Ni<sub>19</sub>Cu<sub>12</sub>Co<sub>19</sub> HEA cooled to room temperature

Stable phases	Constituent elements	Amount in mole (%)	Temperature range (°C)
BCC_B2	Ni,Co:Ti,Al:VA	69.6	≈ 1276 – $T_{room}$
FCC-L2 <sub>1</sub>	Cu:Cu:VA	13.1	≈ 966 – $T_{room}$
HEUSLER_L2 <sub>1</sub>	Al:Ti:Co,Ni	6.4	≈ 546 – $T_{room}$
SIGMA	Al,Cr:Nb:Nb	4.6	≈ 445 – $T_{room}$
C15-LAVES	Cr:Nb	6.3	≈ 176 – $T_{room}$
O_PHASE	Ti:Al:Nb	0.09	≈ 56 – $T_{room}$

The predominant phases obtained – BCC and FCC can serve as a good balance for high-temperature strength, hardness and ductility [16,30]. Also, the incorporation of the Heusler phase as a paramagnetic variant is capable of inciting high mechanical strength at elevated temperatures [31]. Upon careful introduction of the Sigma and Laves phases, the wear properties and corrosion inhibition behaviour of the HEAs can be enhanced [32,33]. Generally, intermetallic-containing alloys benefit from lightweightness, great specific strength, elevated temperature and corrosion resistance capabilities that find application in the aerospace, energy storage and automotive to mention but a few [15–17].

### 3.3 Thermodynamic simulation of the mechanical properties of Ti<sub>20</sub>Al<sub>20</sub>Cr<sub>5</sub>Nb<sub>5</sub>Ni<sub>19</sub>Cu<sub>12</sub>Co<sub>19</sub> HEA

The Property Model Calculation (PMC) module of the ThermoCalc software was employed in the simulation of the mechanical properties of the designed HEA. More specifically, as a function of temperature, the total hardness property of the HEA was predicted.

A phenomenological trend in Figure 3 shows an increase in the hardness property of the HEA as temperature increases. BCC\_B2 occupying more than half of the phase constituent was considered as the matrix phase in the entire simulation process. The BCC\_B2 is characteristic of high-temperature stability and enhanced hardness as corroborated in Figure 2, where its stability is maintained over a wide range of temperatures. The inherent properties of the BCC\_B2 phase is responsible for their extensive application in aerospace, refractory and potentially in nuclear reactors [30,34].

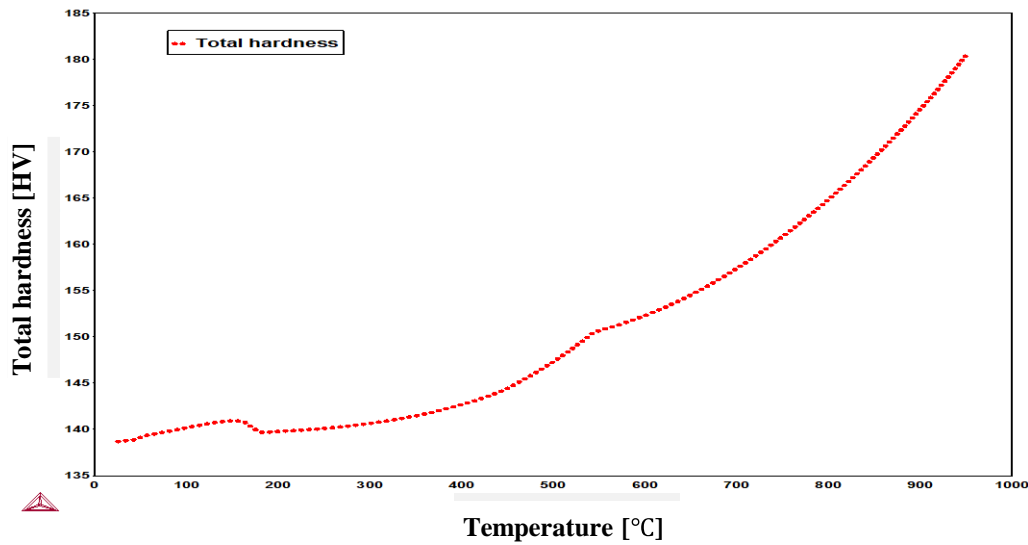


**Fig. 3:** Predicted total hardness of non-equitoxic  $Ti_{20}Al_{20}Cr_5Nb_5Ni_{19}Cu_{12}Co_{19}$  HEA

The trending increase in hardness with temperature as observed in Figure 3 explains a situation of the fabrication process other than the behaviour of the material in service. For example, during the spark plasma sintering process, investigations from the literature report that an increase in the sintering temperature translates to higher hardness of the sintered profile [35–37]. This anomaly is unexpected in materials during service where the intrinsic hardness property of the material in service is expected to decrease as the temperature increases due to the weakening of the material’s intermolecular bonding.

In Figure 4, the Heat map and 3D-surface plot show the total hardness of the HEA at ambient temperature predicted to be 144.1 HV.

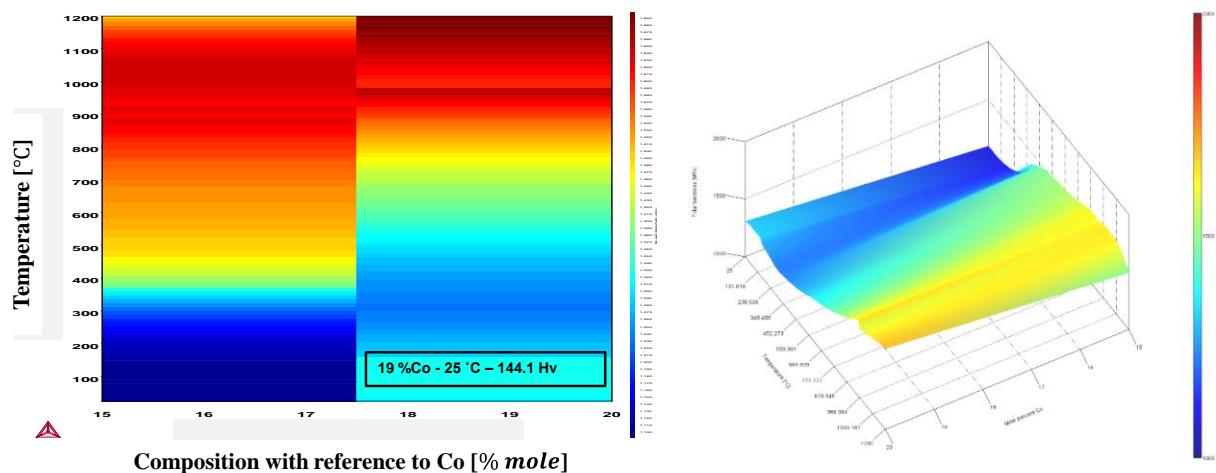


**Fig. 4:** Heat map and 3D-surface plot showing the predicted total hardness of non-equitoxic  $Ti_{20}Al_{20}Cr_5Nb_5Ni_{19}Cu_{12}Co_{19}$  HEA

## 4. Conclusion

Prediction of thermodynamic parameters, phase features and mechanical properties brewed from thermo-physical calculations and ThermoCalc simulation was performed in the design of  $\text{Ti}_{20}\text{Al}_{20}\text{Cr}_5\text{Nb}_5\text{Ni}_{19}\text{Cu}_{12}\text{Co}_{19}$  HEA. Results from the thermo-physical parametric calculation and ThermoCalc show that the HEA, a multi-phased system is a low-density ( $6.22 \text{ gcm}^{-3}$ ) class of HEA with 6.88 VEC value and a predicted total hardness of 144.1 HV. Specifically, BCC, FCC, Laves (C15), Heusler, O-phase and Sigma phases were identified from the thermodynamic simulation with BCC being the predominant phase. The combinatorial properties offered by these phases are capable of delivering lightweightness, high specific strength at elevated temperatures and hardness suitable for the development of components for automotive, aerospace and other industrial applications. The CALPHAD-based technique has a proven record of robustness, reliability and consistency, which can be validated by further studies through experimental characterization and testing following an appropriate production method.

This research was financed by the Special University Research Council (URC) at the University of Johannesburg, South Africa.

## References

- [1] Y.F. Ye, Q. Wang, J. Lu, C.T. Liu, Y. Yang, *Scr. Mater.* **104**, 53–55 (2015).
- [2] J. Yeh, S. Chen, J. Gan, S. Lin, T. Chin, *Metall. Mater. Trans. A.* **35**, 2533–2536 (2004).
- [3] B. Cantor, I.T.H. Chang, P. Knight, A.J.B. Vincent, *Mater. Sci. Eng. A.* **375–377**, 213–218 (2004).
- [4] T.-T. Shun, L.-Y. Chang, M.-H. Shiu, *Mater. Charact.* **81**, 92–96 (2013).
- [5] J.-W. Yeh, *Fundam. Appl.* 1–19 (2016).
- [6] A. Takeuchi, K. Amiya, T. Wada, K. Yubuta, W. Zhang, A. Makino, *Entropy.* **15**, 3810–3821 (2013).
- [7] X. Yang, Y. Zhang, *Mater. Chem. Phys.* **132**, 233–238 (2012).
- [8] Y. Zhang, X. Yang, P.K. Liaw, *JOM.* **64**, 830–838 (2012).
- [9] S. Guo, C. Ng, J. Lu, C.T. Liu, in: *J. Appl. Phys.* (2011).
- [10] Y. Chen, Y. Li, X. Cheng, C. Wu, B. Cheng, Z. Xu, *Maters. (Basel).* **11** (2018).
- [11] F. Tian, L.K. Varga, N. Chen, J. Shen, L. Vitos, *Intermetallics.* **58**, 1–6 (2015).
- [12] D.B. Miracle, O.N. Senkov, *Acta Mater.* **122**, 448–511 (2017).
- [13] M.H. Tsai, *Entropy.* **18** (2016).
- [14] U.S. Anamu, O.O. Ayodele, E. Olorundaisi, B.J. Babalola, K. Ukoba, N.M. Kibambe, M.C. Umba, T.-C. Jen, P.A. Olubambi, *Manuf. Lett.* **41**, 1708–1715 (2024).
- [15] U.S. Anamu, O.O. Ayodele, E. Olorundaisi, B.J. Babalola, P.I. Odetola, A. Ogunmefun, K. Ukoba, T.-C. Jen, P.A. Olubambi, *J. Mater. Res. Technol.* **27**, 4833–4860, (2023).
- [16] J. Liu, X. Wang, A.P. Singh, H. Xu, F. Kong, F. Yang, *Metals (Basel).* **11** (2021).
- [17] M. Morinaga, Elsevier, 2019.
- [18] A. Kumar, M. Gupta, *Metals (Basel).* **6** (2016).
- [19] R. Feng, M.C. Gao, C. Lee, M. Mathes, T. Zuo, S. Chen, J.A. Hawk, Y. Zhang, P.K. Liaw, *Entropy.* **18**, 333 (2016).
- [20] D.B. Miracle, J.D. Miller, O.N. Senkov, C. Woodward, M.D. Uchic, J. Tiley, *Entropy.* **16**, 494–525 (2014).
- [21] F.M. AL-Oqla, M.S. Salit, 4 - Material selection for composites, in: F.M. AL-Oqla, M.S.B.T.-M.S. for N.F.C. Salit (Eds.), Woodhead Publishing. **73–105** (2017).
- [22] S.R. Oke, O.E. Falodun, A. Bayode, U.S. Anamu, P.A. Olubambi, *J. Alloys Compd.* **968**, 172030, (2023).
- [23] E. Olorundaisi, B.J. Babalola, M.L. Teffo, U.S. Anamu, P.A. Olubambi, J. Fayomi, A.O. Ogunmefun, *Discov. Nano.* **18(1)**, 117 (2023).
- [24] J.W. Yeh, S.K. Chen, S.J. Lin, J.Y. Gan, T.S. Chin, T.T. Shun, C.H. Tsau, S.Y. Chang, *Adv. Eng. Mater.* **6**, 299–303 (2004).
- [25] M.G. Poletti, L. Battezzati, *Acta Mater.* **75**, 297–306 (2014).
- [26] Y. Zhang, X. Yang, P.K. Liaw, *Jom.* **64**, 830–838 (2012).
- [27] Y. Zhang, Y.J. Zhou, J.P. Lin, G.L. Chen, P.K. Liaw, *Adv. Eng. Mater.* **10**, 534–538 (2008).
- [28] C. Zhang, F. Zhang, S. Chen, W. Cao, *JOM.* **64**, 839–845 (2012).
- [29] P. Martin, C.E. Madrid-Cortes, C. Cáceres, N. Araya, C. Aguilar, J.M. Cabrera, *Comput. Phys. Commun.* **278**,

- 108398 (2022).
- [30] F. Liu, P.K. Liaw, Y. Zhang, *Metals (Basel)*. **12** (2022).
  - [31] Z. Wen, Y. Zhao, H. Hou, B. Wang, P. Han, *Mater. Des.* **114**, 398–403 (2017).
  - [32] M.-H. Chuang, M. Tsai, C.-W. Tsai, N.-H. Yang, S.-Y. Chang, J.-W. Yeh, P.-H. Lee, S.-J. Lin, *J. Alloys Compd.* **551**, 12–18 (2013).
  - [33] J.B. Cheng, X.B. Liang, B.S. Xu, *Surf. Coatings Technol.* **240**, 184–190 (2014).
  - [34] X. Chang, M. Zeng, K. Liu, L. Fu, *Adv. Mater.* **32** (2020).
  - [35] U.S. Anamu, E. Olorundaisi, O.O. Ayodele, B.J. Babalola, P.I. Odetola, A. Ogunmefun, K. Ukoba, T. Jen, P.A. *Mater. Sci. Forum*, **1116**, 85–94 (2024).
  - [36] V.P. Mkhwanazi, B.J. Babalola, O.O. Ayodele, E. Olorundaisi, U.S. Anamu, P.I. Odetola, N.M. Kibambe, T. Madzivhandila, P.A. Olubambi, *Mater. Today Proc.* (2023).
  - [37] E. Olorundaisi, B.J. Babalola, U.S. Anamu, M.L. Teffo, N.M. Kibambe, A.O. Ogunmefun, P. Odetola, P.A. Olubambi, *Manuf. Lett.* **41**, 160–169 (2024).